Correlation between mechanical properties and ionic conductivity of polycrystalline sodium superionic conductors: a relative density-dominant relationship

Eric Jianfeng Cheng[1]*, Tao Yang[1,2], Yuanzhuo Liu[1,2], Linjiang Chai[2], Regina Garcia-Mendez[3], Eric Kazyak[4], Zhenyu Fu[5], Guoqiang Luo[5], Fei Chen[5], Ryoji Inada[6], Vlad Badilita[7], Huanan Duan[8], Ziyun Wang[9], Jiaqian Qin[10], Hao Li[1], Shin-ichi Orimo[1,11], Hidemi Kato[11]

[1]Advanced Institute for Materials Research (WPI-AIMR), Tohoku University, Sendai 980-8577, Japan; [2]College of Materials Science and Engineering, Chongqing University of Technology, Chongqing 400054, China; [3]Department of Materials Science and Engineering, Johns Hopkins University, Baltimore, MD 21218 USA; [4]Department of Mechanical Engineering, University of Wisconsin-Madison, Madison, WI, 53706, USA; [5]State Key Laboratory of Advanced Technology for Materials Synthesis and Processing, Wuhan University of Technology, Wuhan 430070, China; [6]Department of Electrical and Electronic Information Engineering, Toyohashi University of Technology, Toyohashi 441-8580, Japan; [7]Institute of Microstructure Technology, Karlsruhe Institute of Technology, Eggenstein-Leopoldshafen 76344, Germany; [8]State Key Laboratory of Metal Matrix Composites, School of Materials Science and Engineering, Shanghai Jiao Tong University, Shanghai 200240, China; [9]School of Chemical Sciences, University of Auckland, Auckland 1010，New Zealand; [10]Metallurgy and Materials Science Research Institute, Chulalongkorn University, Bangkok 10330, Thailand; [11]Institute for Materials Research, Tohoku University, Sendai 980-8577, Japan

*Correspondence: ericonium@tohoku.ac.jp

Abstract

Sodium superionic conductors (NASICON) are pivotal for the functionality and safety of solid-state sodium batteries. Their mechanical properties and ionic conductivity are key performance metrics, yet their correlation remains inadequately understood. Addressing this gap is vital for concurrent enhancements in both properties. This study summarizes recent literature on the sintered polycrystalline NASICON solid electrolyte $Na_{1+x}Zr_2Si_xP_{3-x}O_{12}$ (NZSP, $0 \leq x \leq 3$), focusing on its mechanical properties and ionic conductivity, and identifies a positive correlation between these properties at ambient temperatures. Microstructural analysis reveals

that a range of factors, including relative density, grain size, secondary phases, and crystal structures, significantly influence the properties of NZSP. Notably, an increase in relative density uniquely contributes to simultaneous enhancements in both hardness and ionic conductivity. Consequently, future research should prioritize enhancing the relative density of NZSP, potentially by employing advanced sintering techniques such as spark plasma sintering (SPS) and microwave-assisted sintering. The correlation between mechanical properties and ionic conductivity observed in NZSP is also evident in other oxide solid electrolytes, such as garnet $Li_7La_3Zr_2O_{12}$ (LLZO). This investigation not only suggests a potential linkage between these crucial properties but also guides subsequent strategies for refining polycrystalline oxide solid electrolytes for advanced battery technologies.

1. Introduction

In the early 21st century, environmental considerations have gained increasing importance, profoundly influencing economic progression and human sustainability. The implementation of international agreements such as the Kyoto Protocol and the Paris Agreement signifies a collective global commitment to diminishing carbon emissions, catalyzing a shift from traditional fossil fuels to renewable energy sources. This transformation is imperative in addressing climate change and promoting sustainable development.

The inherent intermittency of renewable energy sources, such as solar and wind, necessitates the integration of reliable electrochemical energy storage systems into future electrical grids. These systems are pivotal in managing this intermittency and ensuring a stable energy supply. The main energy storage technologies include lead-acid, nickel-cadmium (Ni-Cd), nickel-metal hydride (NiMH), lithium-ion, and sodium-sulfur (Na-S) batteries [1]. Among these, sodium-ion batteries (NIBs) stand out due to their cost-effectiveness and reliable performance, garnering significant attention in both academia and industry [2, 3].

A critical aspect of battery technology is safety, an area where solid electrolytes (SEs) demonstrate considerable promise. Traditional organic liquid electrolytes are susceptible to leakage [4], electrode corrosion [5], and risks of combustion and explosion under high temperatures [6]. In contrast, inorganic SEs can fundamentally mitigate these safety issues,

elevating the overall safety profile of batteries due to their non-volatility, mechanical and thermal stability, and low flammability [2, 3, 7-9]. Additionally, SEs perform dual functions as both electrolytes and separators, which could simplify battery architecture and reduce packaging costs [10]. As a result, research on SEs has emerged as a focal point in the advancement of secondary battery technologies.

The historical development of SEs can be traced back to the early 19th century. Michael Faraday's seminal discovery of the cation conductor Ag_2S and anion conductor PbF_2 in 1830, which demonstrated metal-like ionic conductivity at elevated temperatures (177-500 °C), laid the foundational groundwork for the field of solid-state ionics (SSI). In 1884, Emil Warburg extended Faraday's principles, establishing the Na^+ transport number as unity in his experiments using Thuringer glass [11]. Subsequently, Walther Nernst made significant contributions by formulating the Nernst equation around 1889. A breakthrough was achieved in 1914, when Carl Tubandt and Erich Lorenz discovered the high Ag^+ conductivity in α-AgI, leading to the exploration of AgI-type solid electrolytes [12, 13]. This pioneering work was further advanced in 1923 with the discovery of monoclinic, halogen-containing SEs, exemplified by Li^+ conductor $LiAlCl_4$, marking a notable progression in SSI. In the subsequent period, notably in the 1930s, research focused on substituting halogen elements in the composition of LiX (X= F, Cl, Br, I) to enhance their room temperature (RT) Li^+ conductivity [14].

The trajectory of SE development took a significant turn in 1966 with the introduction of the Ag_3SI solid electrolyte, which exhibited considerable Ag^+ conductivity of 10 mS/cm at RT. This development was crucial as it led to the assembly of a solid-state cell $Ag/Ag_3SI/I_2$, effectively addressing the flammability issue associated with organic liquid electrolytes [15-18]. Further advancements were made in 1967 with the β-alumina electrolyte ($Na_2O{\cdot}11Al_2O_3$), recognized for its high Na^+ conductivity (10^6 mS/cm at 300 ºC) and its application in Na-S batteries [19, 20]. A pivotal breakthrough occurred in 1976 when Hong and Goodenough synthesized a promising Na^+ inorganic SE, $Na_{1+x}Zr_2Si_xP_{3-x}O_{12}$ (NZSP, $0 \leq x \leq 3$) [21]. NZSP, a solid solution derived from $NaZr_2P_3O_{12}$ (NZP) and $Na_4Zr_2Si_3O_{12}$ (NZS), with Si partially substituting for P to maintain charge balance, has garnered considerable attention due to its high RT ionic conductivity (up to 0.67 mS/cm), stable three-dimensional structure, wide

electrochemical window (>5V *vs.* Na/Na^+), high thermal stability, compatibility with a Na metal anode, and moisture insensitivity [2, 22, 23]. However, its RT ionic conductivity fell short of practical application requirements of ≥1.0 mS/cm. Consequently, enhancing the RT ionic conductivity of NZSP has become a central focus of contemporary research. Since the 1980s, various studies have reported significant progress in this area through the optimization of processing conditions (e.g., modifying sintering parameters, incorporating sintering aids, employing novel sintering techniques) and composition (e.g., adjusting the *x* value and ionic doping). Recent advancements have greatly improved the RT ionic conductivity of NZSP to 1.0 mS/cm [10, 24-28]. In 1990, a direct analogue of NZSP, $Li_{1.3}Al_{0.3}Ti_2(PO_4)_3$ (LATP), was discovered [29]. Beginning in the late 2010s, the research emphasis shifted towards integrating NASICON solid electrolytes into all-solid-state batteries. The most significant challenge has been addressing the interfacial contact issue between solid electrolytes and electrodes [30, 31]. Fig. 1 succinctly captures the developmental history of NZSP, illustrating the chronological advancements in this evolving field.

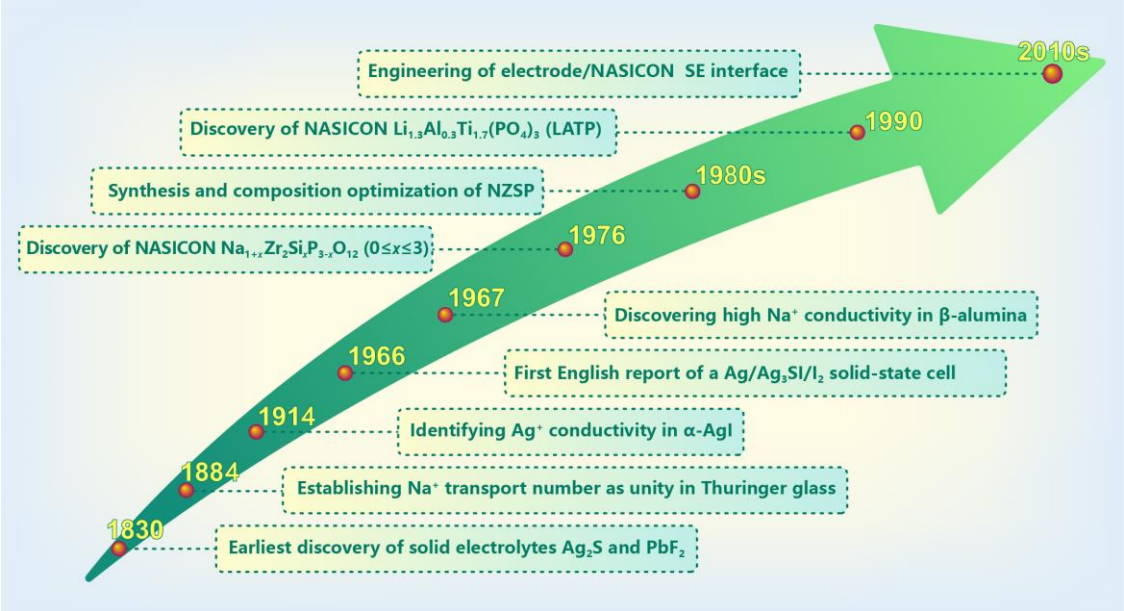

Fig. 1. A succinct history of NASICON solid electrolyte NZSP

Recent studies have underscored the limitations of focusing exclusively on high ionic conductivity to ensure the long-term stability and safety of sodium batteries using NASICON solid electrolytes. These electrolytes will inevitably encounter challenges such as metal dendrite growth and crack formation in practical applications, leading to electrolyte failure [27, 32].

Addressing these challenges necessitates that SEs not only conduct ions but also possess robust mechanical properties, wide electrochemical windows, and chemical stability against electrodes. Specifically, mechanical properties are vital to ensure structural integrity upon cycling, potentially preventing uncontrolled penetration of metal dendrites, thus maintaining battery safety and performance [2, 33-36].

The formation of metal dendrites within SEs is a complex phenomenon that extends beyond the scope of classical mechanics. Monroe et al. proposed that the growth of metal dendrites could be effectively mitigated by ensuring that the shear modulus of the SEs is at least twice that of the metallic anodes [37]. However, experimental studies have extensively demonstrated metal dendrite formation in ceramic SEs, even where the shear modulus markedly surpasses that of the metallic anodes [38-40]. In addition, the role of electronic conductivity within SEs has been identified as a critical factor influencing metal dendrite growth [41]. Despite these complexities, enhancing the mechanical properties of SEs remains a viable strategy for the physical suppression of metal dendrite growth in SEs. Practical strategies include minimizing surface cracks and flaws through meticulous polishing and reducing pore presence by optimizing sintering conditions.

The mechanical properties of NZSP are also crucial for the manufacturing and performance of NZSP-based solid-state batteries (SSBs). For example, the operation of SSBs benefits from a higher fracture toughness in electrolytes, as it allows the use of thinner layers, thereby reducing resistance and enhancing energy density. Furthermore, empirical evidence indicates a positive correlation between fracture toughness and critical current density, with the critical current density increasing with the fracture toughness [42]. Additionally, mitigating micro-cracking in SEs has been found to correlate with the improvement in ductility [43]. Research on the mechanical properties of NASICON electrolytes has emerged as a critical area for advancing energy storage technologies [10, 24-28, 44-46].

Wolfenstine et al. [47] provided a comprehensive summary of the primary mechanical properties of sintered polycrystalline NZSP, which include hardness (4.4-4.9 GPa), elastic modulus (56-97 GPa), fracture toughness (1-1.5 $MPa \cdot m^{0.5}$), and fracture strength (50-110 MPa). Recent investigations have broadened our understanding of these properties, enriching the data

pool necessary for establishing a correlation between mechanical properties and ionic conductivity.

In the pursuit of high-performance solid-state batteries, the manufacturing of SEs that exhibit superior mechanical properties and ionic conductivity is paramount. Despite advancements in developing NZSP electrolytes with improved mechanical properties and ionic conductivity through various methods, a comprehensive examination of strategies to enhance both attributes concurrently remains lacking. This study addresses two fundamental inquiries: the existence of a direct correlation between the mechanical properties and ionic conductivity of NASICON SEs, and the strategies for concurrent improvement of these properties in future research. Through an extensive analysis of existing experimental data, this work elucidates key parameters indicative of these properties and explores their interrelationship. The findings provide valuable insights for the future development of sintered polycrystalline SEs with optimized overall performance.

2. Mechanical properties of sintered polycrystalline NZSP

The mechanical properties of NZSP electrolytes, including hardness, elastic modulus, and fracture toughness, are crucial in preventing crack propagation, suppressing dendrite growth, and maintaining a stable interface with a Na metal anode [47]. Consequently, NZSP must not only possess high ionic conductivity but also adequate mechanical properties to guarantee operational stability. Recently, an increasing number of studies have simultaneously investigated both the mechanical properties and ionic conductivity of NZSP. This integrative approach is significant as it offers a more holistic understanding of SE performance. Despite growing interest, research directly exploring the interplay between these critical properties remains notably scarce. Table 1 provides a comprehensive overview of the existing experimental data, effectively contrasting the mechanical properties with the ionic conductivity of NZSP electrolytes.

In reviewing the research progress on NZSP electrolytes, it is noteworthy that Nonemacher et al. initially characterized their mechanical properties in 2019 [24]. This seminal work has catalyzed a growing interest in the field, evidenced by a consistent annual increase in related research. The predominant strategies to enhance the mechanical properties of NZSP encompass

a variety of approaches: doping [24-26], compositional modification [10], incorporation of sintering aids [27], and use of novel processing techniques such as microwave-assisted sintering [48] and tape casting-assisted hot-pressing [44]. These methods have been instrumental in improving the mechanical properties of NZSP. Additionally, the ionic conductivity of NZSP at RT reported in the literature spans from 0.1 to 5 mS/cm [2].

Recent studies have increasingly focused on the mechanical properties of sintered polycrystalline NZSP, with specific attention to hardness [10, 24-28, 44], elastic modulus [24, 25, 27, 28], bending strength [10], and fracture toughness [24, 28]. Notably, the latest measurements for hardness and elastic modulus exceed the ranges previously summarized by Wolfenstine et al. [47] in 2022, which were 4.4-4.9 GPa for hardness and 56-97 GPa for elastic modulus. Furthermore, the literature reveals significant variations in the reported mechanical properties and ionic conductivity, yet a definitive correlation between these parameters remains elusive. Given that hardness is a fundamental mechanical property of NASICON electrolytes, which positively correlates with the elastic modulus [47] and is comparatively simpler to measure than other mechanical properties, it has become a primary focus of this research. Moreover, the hardness of a sintered polycrystalline NZSP serves as an indicator of its relative density, which in turn is fundamentally associated with its ionic conductivity. As a result, this study aims to elucidate the relationship between hardness and total ionic conductivity of sintered polycrystalline NZSP at RT, thereby shedding light on the interplay between the mechanical properties and ionic conductivity of NASICON SEs.

Table 1 Mechanical properties and total ionic conductivity of sintered polycrystalline NZSP at RT

Compound	Sintering condition	Secondary phase/impurity	Grain size (μm)	Relative density (%)	Mechanical properties						Total ionic conductivity at RT (mS/cm)	Ref.
$Na_3Zr_2Si_2PO_{12}$	1200 °C-0.5 h +1150 °C-5 h	ZrO_2	/	85~93	Vickers Hardness (HV)	734.7	Elastic Modulus (GPa)	88	Fracture Toughness ($MPa·m^{1/2}$)	1.5	1.7	Nonemacher et al. 2019 [24]
$Na_{3.1}Al_{0.05}Y_{0.05}Zr_{1.9}Si_2PO_{12}$						693.9		83		1.55	1.6	
$Na_{3.2}Al_{0.1}Y_{0.1}Zr_{1.8}Si_2PO_{12}$						561.2		73		1.59	1.3	
$Na_{3.4}Al_{0.2}Y_{0.2}Zr_{1.6}Si_2PO_{12}$						673.5		75		1.58	1.4	
$Na_{3.6}Al_{0.3}Y_{0.3}Zr_{1.4}Si_2PO_{12}$						602.0		79		1.35	0.46	
$Na_3Zr_2Si_2PO_{12}$	1050 °C-12 h	$Na_2ZrSi_2O_7$, ZrO_2, SiO_2	/	92.4	Vickers Hardness (HV)	232.7	Young's Modulus (GPa)	54.4	/		0.285	Luo et al. 2022 [25]
$Na_{3+x}Zr_{1.9}Co_{0.1}Si_2PO_{12}$		$Na_2ZrSi_2O_7$, ZrO_2		90.9		163.5		48			0.333	
$Na_{3+x}Zr_{1.8}Co_{0.2}Si_2PO_{12}$		$Na_2ZrSi_2O_7$, ZrO_2		86.6		143.6		37			0.389	
$Na_{3+x}Zr_{1.7}Co_{0.3}Si_2PO_{12}$		$Na_2ZrSi_2O_7$, ZrO_2, SiO_2, $Na_6Si_2O_7$		85.6		137.3		36			0.457	
$Na_{3+x}Zr_{1.9}Fe_{0.1}Si_2PO_{12}$		$Na_2ZrSi_2O_7$, ZrO_2		92.8		244.5		60			0.372	
$Na_{3+x}Zr_{1.8}Fe_{0.2}Si_2PO_{12}$		$Na_2ZrSi_2O_7$, ZrO_2		92.8		454.2		79			0.390	
$Na_{3+x}Zr_{1.7}Fe_{0.3}Si_2PO_{12}$		$Na_2ZrSi_2O_7$, ZrO_2		93.1		510.6		80.3			0.513	
$Na_{3+x}Zr_{1.9}Ni_{0.1}Si_2PO_{12}$		$Na_2ZrSi_2O_7$		89.3		103.7		38			0.558	
$Na_{3+x}Zr_{1.8}Ni_{0.2}Si_2PO_{12}$		$Na_2ZrSi_2O_7$, ZrO_2		85.2		110.9		37.5			0.443	
$Na_{3+x}Zr_{1.7}Ni_{0.3}Si_2PO_{12}$		$Na_2ZrSi_2O_7$, ZrO_2, SiO_2, $Na_6Si_2O_7$, $Ni_3(PO_4)_2$		85.4		119.0		38			0.113	
$Na_3Zr_2Si_2PO_{12}$	1250 °C-1 h	Amorphous phase, ZrO_2	0.5–3	92.1	Bend Strength (MPa)	73	/				0.51	Go et al. 2021 [10]
$Na_{3.1}Zr_{1.55}Si_{2.3}P_{0.7}O_{11}$		Amorphous phase, ZrO_2	2–6	91.7		95					1.4	
$Na_3Zr_2Si_2PO_{12}$	1100 °C-12 h	ZrO_2	＞1	88.4	Vickers Hardness (HV)	291	/				0.39	Ran et al. 2021 [26]
$Na_{3.1}Zr_{1.8}Sc_{0.1}Ge_{0.1}Si_2PO_{12}$			＜1	91.1		/					1.61	

$Na_{3.125}Zr_{1.75}Sc_{0.125}Ge_{0.125}Si_2PO_{12}$				99.7		505					4.64	
$Na_{3.15}Zr_{1.7}Sc_{0.15}Ge_{0.15}Si_2PO_{12}$				95.7		/					1.89	
$Na_3Zr_2Si_2PO_{12}$	1180 °C-12 h	/	1.4	86.7	Vickers Hardness (HV)	346.9	Young's Modulus (GPa)	55.5	/		0.61	Gao et. al. 2022 [27]
$Na_3Zr_2Si_2PO_{12}$+2 wt% TiO_2		TiO_2	1.9	95.9		949.0		92.2			0.66	
$Na_3Zr_2Si_2PO_{12}$	1050 °C-5 min (SPS)	$Na_2ZrSi_4O_{11}$, $ZrSiO_4$, SiO_2	/	90	Vickers Hardness (HV)	673.5	Elastic Modulus (GPa)	82	Fracture Toughness ($MPa \cdot m^{1/2}$)	2.1	0.34	Hitesh et al. 2023 [28]
	1050 °C-10 min (SPS)		/	94		357.1		77		2.8	0.35	
	1050 °C-20 min (SPS)		17	97.4		540.8		81		2.3	0.45	
	1050 °C-20 min (SPS)+1100 °C-5 h (annealing)	$Na_2ZrSi_4O_{11}$	46	97.9		469.4		81.5		1.9	/	
	1050 °C-20 min (SPS)+1100 °C-10 h (annealing)	$Na_2ZrSi_4O_{11}$	42	98		510.2		79.9		1.8	/	
	1050 °C-20 min (SPS)+1100 °C-20 h (annealing)	$Na_2ZrSi_4O_{11}$	52	96.1		693.9		86.7		2.6	/	
	1050 °C-20 min (SPS)+1100 °C-40 h (annealing)	$Na_2ZrSi_4O_{11}$	71	96.5		581.6		84.8		2.2	/	
$Na_{3.16}Zr_{1.84}Y_{0.16}Si_2PO_{12}$	1200 °C-10 h (hot-pressing)	Na_3PO_4、ZrO_2	<1	90	Vickers Hardness (HV)	325	/		/		0.1	Naranjo-Balseca et al. 2023 [44]

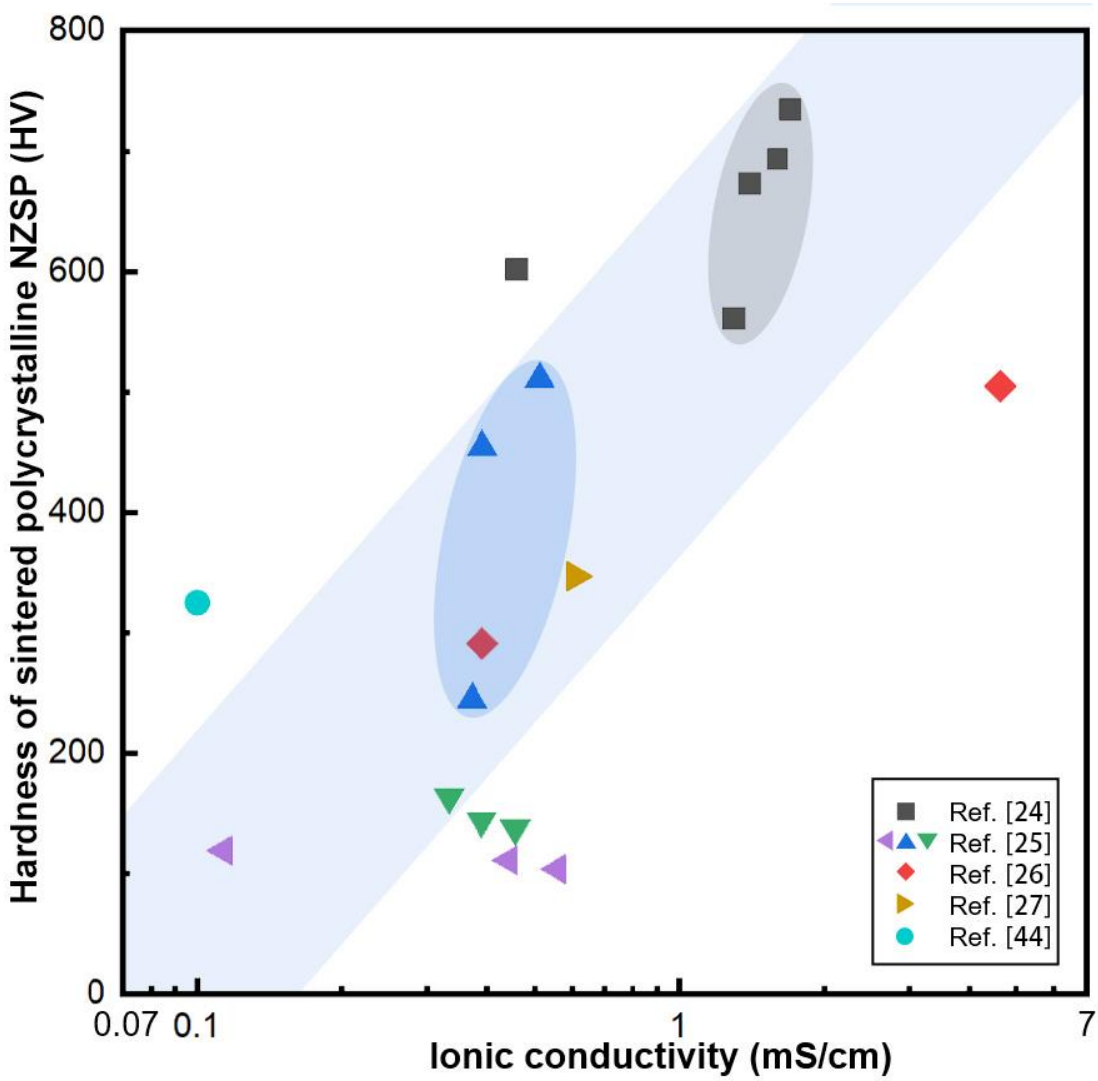

Fig. 2 Correlation between total ionic conductivity and hardness of sintered polycrystalline NZSP at RT. The data are sourced from references [24-27, 44]. Identical symbols indicate samples obtained by varying a specific condition to achieve different ionic conductivities and hardnesses. The gray squares represent doping with varying contents of Al and Y [24]; purple, blue, and green triangles represent doping with varying amounts of Ni, Fe, and Co, respectively [25]; red diamonds represent doping with Sc and Ge [26]. Hardness conversion: HV×9.8=GPa×1000.

In Fig. 2, a comparative analysis of the interrelationship between the total ionic conductivity and hardness of sintered polycrystalline NZSP is presented. This plot illustrates a

predominant trend where an enhancement in ionic conductivity corresponds to an increase in hardness. This pattern indicates a tentative positive correlation between the ionic conductivity and the hardness of sintered polycrystalline NZSP. It is also worth noting that NZSP doped with varying amounts of transition metals of Ni and Co, exhibited a slight reduction in hardness accompanied by a modest increase in ionic conductivity [25]. This reduction in hardness can be attributed to the gradual decrease in relative density with increasing Co content. Additionally, introducing Ni and Co leads to the formation of secondary phases such as $Na_2ZrSi_2O_7$, which may affect the proposed correlation between mechanical properties and ionic conductivity. The subsequent section will explore the underlying mechanisms that potentially drive the observed positive correlation.

3. Correlation between mechanical properties and ionic conductivity

The intrinsic connection between the mechanical properties and ionic conductivity of polycrystalline NZSP, as briefly discussed earlier, stems from their microstructural characteristics. The mechanical properties are predominantly determined by factors including relative density, the presence of secondary phases, grain size, doping, crystal structure, and bond strength. In parallel, ionic conductivity is similarly influenced by variables such as relative density, crystal structure, sodium ion concentration and mobility, secondary phases, and grain size. This shared dependence on microstructural elements underscores the fundamental correlation between the mechanical and ionic properties of polycrystalline NZSP. The following sections provide an in-depth analysis of trends in mechanical properties and ionic conductivity, emphasizing their microstructural foundations. Moreover, the study highlights various measures, such as processing techniques, doping methods, and sintering aids, that impact these properties. The aim is to provide a comprehensive guide for future research endeavors seeking to synergistically enhance both the mechanical properties and ionic conductivity of NASICON

SEs.

3.1 Relative density

Relative density significantly influences the mechanical properties of NZSP. A higher relative density corresponds to reduced pore defects and more compact grain contact, thereby diminishing the likelihood of material fracture due to stress concentration under loading conditions. This enhancement in relative density also promotes a more efficient flow of sodium ions, leading to increased ionic conductivity. SEM microstructures depicted in Fig. 3 demonstrate that with an increase in relative density, there is a concurrent rise in both hardness and ionic conductivity of the sintered polycrystalline NZSP. Therefore, future research should focus on improving the relative density of sintered polycrystalline NZSP, as this could synergistically enhance both aforementioned properties. In an optimal scenario, both the hardness and ionic conductivity of a polycrystalline NZSP are expected to approach the properties of a single crystalline NZSP as the relative density reaches 100% and the boundary resistance is reduced to zero. It is also important to note that hard crystalline oxide SEs generally demonstrate significantly higher ionic conductivity compared to their softer amorphous counterparts [49, 50].

The conventional preparation method, i.e., high-temperature and pressure-less sintering, is straightforward and scalable. However, they often result in NZSP electrolytes characterized by a high concentration of defects, such as pores, yielding relatively low relative densities around 90% [28]. High-energy ball-milling enhances the densification of NZSP pellets during sintering, but this approach concurrently introduces disordering and partial amorphization to the particle surface [51]. In response to this challenge, research has shifted towards exploring alternative processing methods for polycrystalline NZSP. Techniques such as sol-gel which facilitates uniform precursor mixing at the molecular level, and spark plasma sintering (SPS),

known for its rapid densification capabilities through micro-discharges between particles, have successfully produced polycrystalline NZSP with notably high relative densities of approximately 98% and above [28, 52-55]. Moreover, employing a polydisperse particle size distribution in the sintering process can improve the compactness or relative density of sintered polycrystalline NZSP [51].

Furthermore, the inclusion of low-melting-point sintering aids in the precursor mixture has become a common practice for relative density optimization. This strategy leverages the liquid phase formed from the sintering aids to fill gaps among precursor particles. In addition, sintering additives can potentially lower the sintering temperature, modify grain boundary properties, and regulate mass transfer and grain growth. However, most sintering additives have relatively low hardness and ionic conductivity. Consequently, incorporating these additives often decreases the overall hardness and ionic conductivity of the resultant compounds. Nevertheless, using sintering additives can potentially optimize the balance between relative density and secondary phases, thereby enhancing overall mechanical properties and ionic conductivity [56, 57]. In general, densification improves initially as the concentration of sintering aids increases; beyond a certain threshold, it decreases due to the formation of voids. Thus, an optimal content of sintering additives is crucial for promoting mass transport and densification. Sintering additives, such as NaF [58], NaBr [59], Na_3BO_3 [60], $NaPO_3$ [61], Na_2O-Nb_2O_5-P_2O_5 [54], B_2O_3 [62], and La_2O_3 [63], have demonstrated considerable effectiveness in enhancing the relative density of sintered polycrystalline NZSP.

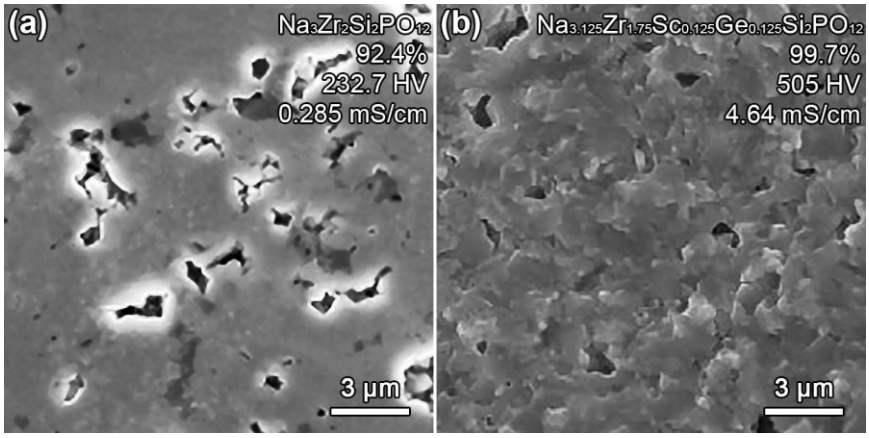

Fig. 3 SEM microstructures of typical sintered polycrystalline NZSP with different relative densities reported in the literature, along with corresponding hardness and ionic conductivity. (a) $Na_3Zr_2Si_2PO_{12}$ and (b) $Na_{3.125}Zr_{1.75}Sc_{0.125}Ge_{0.125}Si_2PO_{12}$. Reprinted with permissions from the studies by Luo et al. [25] and Ran et al. [26].

3.2 Grain sizes

Grain size has a dual impact on the mechanical properties and ionic conductivity of polycrystalline NZSP, presenting a complex "double-edged sword" phenomenon. Enhancing ionic conductivity requires properly increasing the grain size of sintered polycrystalline NZSP, which reduces the volume fraction of grain boundaries that typically exhibit significantly lower ionic conductivity compared to the bulk material. However, excessive grain growth can lead to pore entrapment, detrimental to the densification of NZSP and significantly reducing its mechanical properties and ionic conductivity.

Conversely, although refining grain size improves mechanical properties through grain refinement strengthening, this refinement also increases the volume fraction of grain boundaries. The increase in grain boundaries and associated defects because of grain refinements tends to increase grain boundary resistance and in turn, decrease the overall ionic conductivity of NZSP

[10]. In general, a relatively large average grain size is preferred for sintered polycrystalline SEs.

Given this intricate relationship, precise control over grain size is crucial in balancing the mechanical integrity and ionic conductivity of sintered polycrystalline SEs. Grain size is a direct function of the sintering time, with longer holding times producing larger grains [28]. From the perspective of the sintering process, grain growth occurs through nucleation followed by enlargement. The grain size does not directly impact densification. Grain growth, which involves migration of grain boundaries, is impeded when these boundaries encounter obstacles such as second phases or pores. Therefore, although grain size does not significantly affect densification, the degree of densification does influence grain size.

3.3 Secondary phases

The secondary phases in polycrystalline NZSP play a dual role, similar to grain size in influencing mechanical properties and ionic conductivity. The formation of hard, fine secondary phases like ZrO_2 enhances mechanical strength through secondary phase strengthening. However, the formation of secondary phases often results in a notable reduction in ionic conductivity due to the negligible transport of sodium ions through these secondary phases. This decrease is attributed to the generally low ionic conductivity of the secondary phases and the introduction of new grain boundary resistance [10]. Typical secondary phases in sintered polycrystalline NZSP include ZrO_2, SiO_2, $Na_2ZrSi_4O_{11}$, $ZrSiO_4$, $Na_6Si_2O_7$, and some amorphous phases [25, 28, 52]. These phases predominantly arise from incomplete crystallization during sintering. This incomplete crystallization process, often caused by the volatilization of Na and P elements at high temperatures, results in a deviation from the stoichiometric $Na_3Zr_2Si_2PO_{12}$, leading to new phase formation. While these impurity phases can enhance mechanical properties, they can also cause microcracking in sintered NZSP, particularly due to stress

concentration during the post-sintering cooling process [10].

To mitigate the formation of these secondary phases, two primary strategies are currently employed. The first involves adding excessive Na and P elements, such as Na_2CO_3 [27], $(NH_4)_2HPO_4$ [25], or Na_3PO_4 [28], and covering the green pellets with NZSP powder during conventional sintering [44]. The second strategy includes adopting novel processes that lower sintering temperatures, thus reducing the volatilization of Na and P. These include SPS [53, 54] and microwave sintering [48]. Both approaches have successfully lowered the processing temperature by approximately 250 °C, significantly minimizing the likelihood of secondary-phase formation [52-54, 64]. Meanwhile, the composition of the secondary phases can be precisely regulated through the incorporation of targeted sintering additives or elemental dopants. For example, La_2O_3 was used as a sintering aid to modulate the chemical composition at the grain boundaries and induce the formation of the secondary phase $Na_3La(PO_4)_2$, which not only increased the ionic conductivity but also enhanced the relative density of sintered polycrystalline NZSP [63]. Similarly, the introduction of Al into the Si/P sites led to an increased formation of the secondary phase Na_3PO_4 at the grain boundary. This resulted in a noticeable decrease in the grain boundary resistance [65].

3.4 Crystal structure

NZSP, characterized by a unique three-dimensional phosphate structure, facilitates fast Na^+ migration. Its formula, $Na_{1+x}Zr_2Si_xP_{3-x}O_{12}$ (where $0 \leq x \leq 3$), varies based on the degree of Si substitution for P. The crystal structure of NZSP shifts with different doping levels of x. Specifically, a rhombohedral structure is observed for $0 \leq x < 1.8$ and $2.2 < x \leq 3$, while a monoclinic phase occurs at $1.8 \leq x \leq 2.2$, as depicted in Fig. 4 [21, 66]. The Zr atoms are coordinated by oxygen atoms forming ZrO_6 octahedra, and silicon and phosphorus (Si/P) atoms are generally surrounded by oxygen atoms forming SiO_4 or PO_4 tetrahedra. The connectivity

between these polyhedra plays a crucial role in the stability and ionic conductivity of the phosphate structure. In the monoclinic phase, the ZrO_6 octahedra and SiO_4/PO_4 tetrahedra connect in a slightly distorted manner compared to the more symmetric rhombohedral phase [67]. As a result, Na^+ ions are coordinated in a more distorted and irregular environment compared to the rhombohedral phase, where the coordination becomes slightly more regular. The change in Na coordination environment influences the ionic conductivity. The rhombohedral phase demonstrates a lower activation energy for Na^+ diffusion, resulting in enhanced ionic conductivity (approximately 0.1-1 mS/cm at RT) [10, 26, 55]. On the other hand, the highest ionic conductivity in monoclinic NZSP, about 0.67 mS/cm, is noted at $x = 2$ [68].

The phase transition between monoclinic and rhombohedral structures in NZSP is not only influenced by Na content but also by temperature. NZSP crystallizes in the monoclinic C2/c space group at RT while transitioning to the rhombohedral phase (R-3c) around 200 ºC [30, 69, 70]. The transition between these crystal structures not only affects ionic conductivity but also mechanical properties. The monoclinic phase, due to its lower symmetry and greater lattice distortion, exhibits slightly increased hardness. The reduced symmetry and increased distortion in the monoclinic structure likely result in a denser crystal lattice, which can enhance atomic packing and bonding interactions within the crystal, leading to greater mechanical rigidity. Nonemacher et al. observed a gradual hardness reduction in NZSP transitioning from the monoclinic to the rhombohedral phase [24]. This suggests a trade-off between mechanical properties and ionic conductivity in polycrystalline NZSP. However, this trade-off may not necessitate compromising the ionic conductivity of the rhombohedral phase for enhanced mechanical properties, as it already exhibits high hardness (5-7 GPa) and elastic modulus (75-85 GPa) [24].

Various methods have been employed to enhance the proportion of the rhombohedral

phase. These include lowering the phase transition temperatures from monoclinic to rhombohedral through Ge doping [71], increasing the stability of the rhombohedral phases via Sc doping [24], and altering the value of x (e.g., x=2.3) to increase the content of the rhombohedral phase [10]. In addition, doping NZSP with various elements can alter the ratio between monoclinic and rhombohedral structures, simultaneously causing changes to the volume of crystal unit cells. These changes significantly affect the mechanical properties and ionic conductivity of NZSP. For example, introducing bivalent elements such as Zn^{2+} and Mg^{2+} [72] or tetravalent elements such as Hf^{4+} [63], increases the rhombohedral phase proportion and enlarges the bottleneck size in Na^{+} migration pathways, facilitating higher Na^{+} mobility. However, when substitutive ions, such as Nd^{3+} and Co^{2+}, have radii substantially larger or smaller than Zr^{4+} (0.72 Å) [73], their integration into the crystal lattice becomes problematic, thereby impeding the enhancement of ionic conductivity [58].

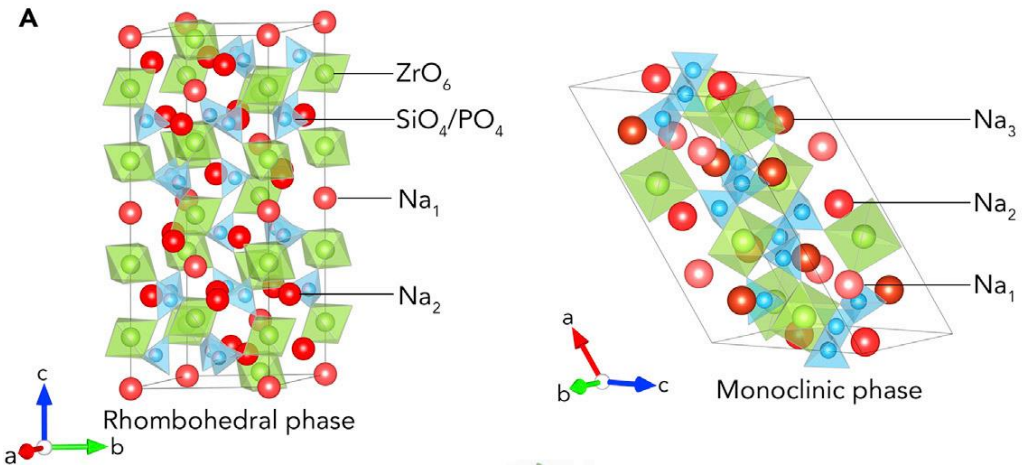

Fig. 4. Two typical crystal structures of NZSP. Reprinted with permission from the study by Lu et al. [74].

3.5 Interplay between hardness and ionic conductivity

Fig. 5 presents an analysis of four key factors influencing the properties of polycrystalline NZSP. This analysis reveals a trade-off relationship between mechanical properties and ionic conductivity for all factors except relative density. The study suggests that enhancing the

relative density of sintered polycrystalline NZSP electrolytes is crucial for simultaneously improving both their mechanical properties and ionic conductivity. Fig. 6 illustrates a positive correlation between density, hardness, and ionic conductivity in sintered polycrystalline NZSP electrolytes. Notably, higher relative densities are consistently linked with increased hardness and ionic conductivity, validating our initial hypothesis. While increasing relative density synergistically enhances these properties, the other three factors predominantly contribute to a trade-off between them. Moreover, these properties exhibit a strong dependence on relative density. Consequently, future research on sintering polycrystalline NZSP should prioritize increasing the relative density. Post-sintering treatments, such as annealing, should optimize the balance between mechanical properties and ionic conductivity.

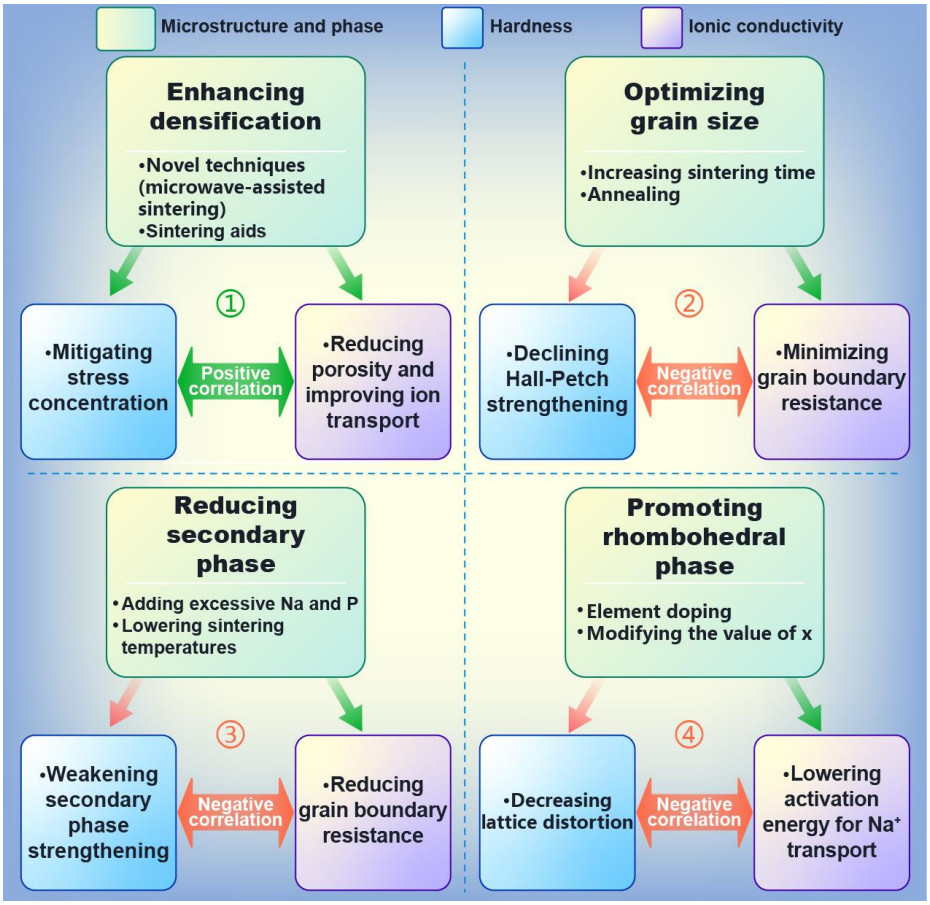

Fig. 5 Summary of key factors influencing both hardness and ionic conductivity of sintered polycrystalline NASICON solid electrolytes.

Furthermore, the correlation between mechanical properties and ionic conductivity observed in polycrystalline NZSP also applies to other high-temperature sintered oxide ceramic electrolytes, such as lithium superionic conductors—LLZO and LATP [75, 76]. For example, as the relative density increased from 85% to 98%, the Vickers hardness of sintered polycrystalline LLZO increased from 4.7 to 9.1 GPa, and the RT ionic conductivity concurrently improved from 0.0094 to 0.34 mS/cm. [76].

3.6 Influence of NZSP mechanical properties on cell performance

The operation of solid-state NIBs will benefit from the higher mechanical properties, particularly the high fracture toughness, of NZSP electrolytes. This increased toughness allows for thinner electrolyte layers, reducing electrolyte resistance and preventing micro-cracking. However, the intrinsic hardness and brittleness of NZSP pose significant challenges and can lead to fractures under mechanical stress, causing battery failure. Additionally, at the interfaces with electrodes, poor contact due to these characteristics can significantly increase interfacial resistance and reduce ionic transfer efficiency, significantly limiting overall cell performance.

Softer Na^+ solid electrolytes, such as the complex hydride $Na_2B_{10}H_{10}$-$Na_2B_{12}H_{12}$, offer solutions similar to those provided by soft halides and sulfide electrolytes in solid-state LIBs [77]. Additionally, incorporating NZSP particles into deformable polymer electrolytes can form ceramic-in-polymer composite solid electrolytes with balanced mechanical properties and ionic conductivity, making them more suitable for practical applications [78, 79]. Moreover, leveraging machine learning in predicting potential Na^+ solid electrolytes beyond NZSP appears highly promising [80].

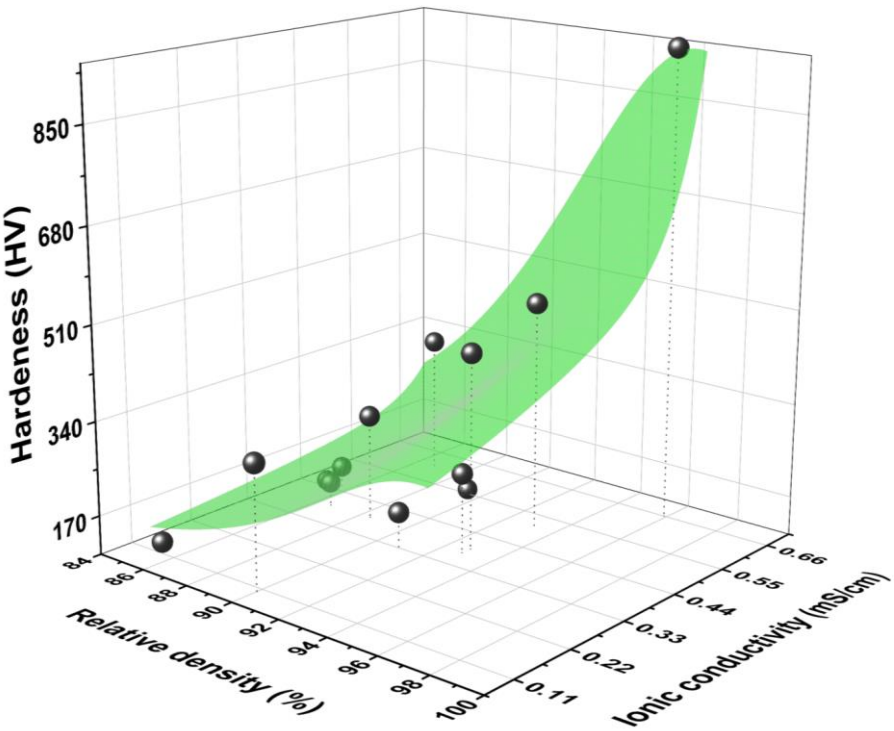

Fig. 6. Correlation of relative densities with ionic conductivity and hardness of sintered polycrystalline NZSP at RT (Data adapted from Refs. [24-27, 44])

4. Conclusion and future perspective

This study investigates the mechanical properties and ionic conductivity of sintered polycrystalline NZSP. An extensive review and analysis of the current literature reveals a generally positive correlation between these two properties, particularly emphasizing the link

between hardness, a major mechanical property, and ionic conductivity. The correlation primarily stems from several factors, including relative density, grain size, secondary phases, and crystal structure. Among these, relative density emerges as the most decisive in determining the relationship between hardness and ionic conductivity. The other factors demonstrate a trade-off effect. Therefore, the advancement of sintered polycrystalline NZSP electrolytes should prioritize enhancing the relative density, leveraging techniques such as SPS, microwave-assisted sintering, and the incorporation of sintering aids. Achieving a high relative density allows for subsequent refinements, e.g., increasing grain size through annealing, to optimize the balance between the mechanical properties and ionic conductivity. The observed correlation between mechanical properties and ionic conductivity in sintered polycrystalline NZSP also applies to sintered polycrystalline oxide lithium superionic conductors, such as LLZO. Advanced characterization techniques, including in-situ nanoindentation and solid-state NMR spectroscopy, combined with computational deep learning methods, can be utilized to further investigate the correlation between mechanical properties and ionic conductivity in sintered polycrystalline solid electrolytes.

Acknowledgments

This research was financially supported by Core Research Cluster for Materials Science (CRC-MS) of Tohoku University, Ensemble Grants for Early Career Researchers 2023 of Tohoku University, GIMRT program of the Institute for Materials Research of Tohoku University (Proposal No. 202308-CRKKE-0221), AIMR Fusion Research program 2023 of the Advanced Institute for Materials Research of Tohoku University, and TEPCO Memorial Foundation.

Data availability

The raw/processed data required to reproduce these findings cannot be shared at this time due

to technical or time limitations.

References

[1] M. Guin, F. Tietz, Survey of the transport properties of sodium superionic conductor materials for use in sodium batteries, Journal of power sources 273 (2015) 1056-1064.

[2] Y. Li, M. Li, Z. Sun, Q. Ni, H. Jin, Y. Zhao, Recent advance on NASICON electrolyte in solid-state sodium metal batteries, Energy Storage Mater. 56 (2023) 582-599.

[3] K.B. Hueso, V. Palomares, M. Armand, T. Rojo, Challenges and perspectives on high and intermediate-temperature sodium batteries, Nano Res. 10(12) (2017) 4082-4114.

[4] H. Chen, J. Liu, X. Zhou, H. Ji, S. Liu, M. Wang, T. Qian, C. Yan, Rapid leakage responsive and self-healing Li-metal batteries, Chemical Engineering Journal 404 (2021) 126470.

[5] P. Du, D. Liu, X. Chen, H. Xie, X. Qu, D. Wang, H. Yin, Research progress towards the corrosion and protection of electrodes in energy-storage batteries, Energy Storage Materials 57 (2023) 371-399.

[6] M. Yuan, K. Liu, Rational design on separators and liquid electrolytes for safer lithium-ion batteries, Journal of Energy Chemistry 43 (2020) 58-70.

[7] E.J. Cheng, Y. Kushida, T. Abe, K. Kanamura, Degradation Mechanism of All-Solid-State Li-Metal Batteries Studied by Electrochemical Impedance Spectroscopy, ACS Appl. Mater. Interfaces 14(36) (2022) 40881-40889.

[8] M. Shoji, E.J. Cheng, T. Kimura, K. Kanamura, Recent progress for all solid state battery using sulfide and oxide solid electrolytes, J. Phys. D: Appl. Phys. 52(10) (2019) 103001.

[9] E.J. Cheng, R. Oyama, T. Abe, K. Kanamura, High-voltage all-solid-state lithium metal batteries prepared by aerosol deposition, J. Eur. Ceram. Soc. 43(5) (2023) 2033-2038.

[10] W. Go, J. Kim, J. Pyo, J.B. Wolfenstine, Y. Kim, Investigation on the Structure and Properties of $Na_{3.1}Zr_{1.55}Si_{2.3}P_{0.7}O_{11}$ as a Solid Electrolyte and Its Application in a Seawater Battery, ACS Appl. Mater. Interfaces (2021) 52727-52735.

[11] E. Warburg, Ueber die Electrolyse des festen Glases, Annalen der Physik 257(4) (1884) 622-646.

[12] C. Tubandt, E. Lorenz, Molekularzustand und elektrisches Leitvermögen kristallisierter Salze, Zeitschrift für Physikalische Chemie 87(1) (1914) 513-542.

[13] K. Funke, Solid State Ionics: from Michael Faraday to green energy—the European dimension, Science and Technology of Advanced Materials 14(4) (2013) 043502.

[14] B. He, F. Zhang, Y. Xin, C. Xu, X. Hu, X. Wu, Y. Yang, H. Tian, Halogen chemistry of solid electrolytes in all-solid-state batteries, Nat. Rev. Chem. (2023) 1-17.

[15] T.T. Vu, H.J. Cheon, S.Y. Shin, G. Jeong, E. Wi, M. Chang, Hybrid electrolytes for solid-state lithium batteries: Challenges, progress, and prospects, Energy Storage Mater. 61 (2023) 102876.

[16] A. Manthiram, X. Yu, S. Wang, Lithium battery chemistries enabled by solid-state electrolytes, Nat. Rev. Mater. 2(4) (2017) 1-16.

[17] H. Tang, Z. Deng, Z. Lin, Z. Wang, I.-H. Chu, C. Chen, Z. Zhu, C. Zheng, S.P. Ong, Probing solid–solid interfacial reactions in all-solid-state sodium-ion batteries with first-principles calculations, Chem. Mater. 30(1) (2018) 163-173.

[18] T. Takahashi, O. Yamamoto, The Ag/Ag3SI/I2 solid-electrolyte cell, Electrochimica Acta 11(7) (1966) 779-789.

[19] Y. Yao, J. Kummer, Ion exchange properties of and rates of ionic diffusion in beta-alumina, J. Inorg. Nucl. Chem. 29(9) (1967) 2453-2475.

[20] G. Tel'Nova, K. Solntsev, Structure and ionic conductivity of a beta-alumina-based solid electrolyte prepared from sodium polyaluminate nanopowders, Inorg. Mater. 51 (2015) 257-266.

[21] H. Hong, J. Kafalas, J. Goodenough, Fast Na^+-ion transport in skeleton structures, Mater. Res. Bull. 11(2) (1976) 203-220.

[22] J. Auborn, D. Johnson Jr, Conductivity of Nasicon ceramic membranes in aqueous solutions, Solid State Ionics 5 (1981) 315.

[23] Z. Zhang, S. Wenzel, Y. Zhu, J. Sann, L. Shen, J. Yang, X. Yao, Y.-S. Hu, C. Wolverton, H. Li, $Na_3Zr_2Si_2PO_{12}$: a stable Na^+-ion solid electrolyte for solid-state batteries, ACS Appl. Energy Mater. 3(8) (2020) 7427-7437.

[24] J.F. Nonemacher, S. Naqash, F. Tietz, J. Malzbender, Micromechanical assessment of Al/Y-substituted NASICON solid electrolytes, Ceram. Int. 45(17) (2019) 21308-21314.

[25] J. Luo, G. Zhao, W. Qiang, B. Huang, Synthesis of Na ion‐electron mixed conductor $Na_3Zr_2Si_2PO_{12}$ by doping with transition metal elements (Co, Fe, Ni), J. Am. Ceram. Soc 105(5) (2022) 3428-3437.

[26] L. Ran, A. Baktash, M. Li, Y. Yin, B. Demir, T. Lin, M. Li, M. Rana, I. Gentle, L. Wang, D.J. Searles, R. Knibbe, Sc, Ge co-doping NASICON boosts solid-state sodium ion batteries' performance, Energy Storage Mater. 40 (2021) 282-291.

[27] Z. Gao, J. Yang, G. Li, T. Ferber, J. Feng, Y. Li, H. Fu, W. Jaegermann, C.W. Monroe, Y. Huang, TiO_2 as Second Phase in $Na_3Zr_2Si_2PO_{12}$ to Suppress Dendrite Growth in Sodium Metal Solid‐State Batteries, Adv. Energy Mater. 12(9) (2022) 2103607.

[28] B. Hitesh, A. Sil, Effect of sintering and annealing on electrochemical and mechanical characteristics of $Na_3Zr_2Si_2PO_{12}$ solid electrolyte, J. Am. Ceram. Soc. (2023) 1–12.

[29] H. Aono, E. Sugimoto, Y. Sadaoka, N. Imanaka, G.y. Adachi, Ionic conductivity of solid electrolytes based on lithium titanium phosphate, Journal of the electrochemical society 137(4) (1990) 1023.

[30] Z. Zhang, Z. Zou, K. Kaup, R. Xiao, S. Shi, M. Avdeev, Y.S. Hu, D. Wang, B. He, H. Li, Correlated migration invokes higher Na^+-ion conductivity in NaSICON-type solid electrolytes,

Advanced Energy Materials 9(42) (2019) 1902373.

[31] Z. Gao, J. Yang, H. Yuan, H. Fu, Y. Li, Y. Li, T. Ferber, C. Guhl, H. Sun, W. Jaegermann, Stabilizing $Na_3Zr_2Si_2PO_{12}$/Na interfacial performance by introducing a clean and Na-deficient surface, Chemistry of Materials 32(9) (2020) 3970-3979.

[32] Y. Zhao, L.V. Goncharova, A. Lushington, Q. Sun, H. Yadegari, B. Wang, W. Xiao, R. Li, X. Sun, Superior Stable and Long Life Sodium Metal Anodes Achieved by Atomic Layer Deposition, Adv. Mater. 29(18) (2017) 1606663.

[33] H. Wan, J.P. Mwizerwa, X. Qi, X. Liu, X. Xu, H. Li, Y.S. Hu, X. Yao, Core-Shell Fe(1-x)S@Na(2.9)PS(3.95)Se(0.05) Nanorods for Room Temperature All-Solid-State Sodium Batteries with High Energy Density, ACS Nano 12(3) (2018) 2809-2817.

[34] H. Wan, W. Weng, F. Han, L. Cai, C. Wang, X. Yao, Bio-inspired Nanoscaled Electronic/Ionic Conduction Networks for Room-Temperature All-Solid-State Sodium-Sulfur Battery, Nano Today 33 (2020) 100860.

[35] G. Liu, X. Sun, X. Yu, W. Weng, J. Yang, D. Zhou, R. Xiao, L. Chen, X. Yao, $Na_{10}SnSb_2S_{12}$: A nanosized air-stable solid electrolyte for all-solid-state sodium batteries, Chem. Eng. J. 420 (2021) 127692.

[36] H. Wan, J.P. Mwizerwa, F. Han, W. Weng, J. Yang, C. Wang, X. Yao, Grain-boundary-resistance-less Na_3SbS_4-Se solid electrolytes for all-solid-state sodium batteries, Nano Energy 66 (2019) 104109.

[37] C. Monroe, J. Newman, The impact of elastic deformation on deposition kinetics at lithium/polymer interfaces, J. Electrochem. Soc 152(2) (2005) A396.

[38] E.J. Cheng, A. Sharafi, J. Sakamoto, Intergranular Li metal propagation through polycrystalline $Li_{6.25}Al_{0.25}La_3Zr_2O_{12}$ ceramic electrolyte, Electrochim. Acta 223 (2017) 85-91.

[39] J. Zhao, Y. Tang, Q. Dai, C. Du, Y. Zhang, D. Xue, T. Chen, J. Chen, B. Wang, J. Yao, In situ observation of Li deposition‐induced cracking in garnet solid electrolytes, Energy Environ. Mater. 5(2) (2022) 524-532.

[40] R. Inada, S. Yasuda, H. Hosokawa, M. Saito, T. Tojo, Y. Sakurai, Formation and stability of interface between garnet-type Ta-doped $Li_7La_3Zr_2O_{12}$ solid electrolyte and lithium metal electrode, Batteries 4(2) (2018) 26.

[41] X. Liu, R. Garcia, A.R. Lupini, Y. Cheng, Z.D. Hood, F. Han, A. Sharafi, J.C. Idrobo, N.J. Dudney, C. Wang, Local electronic structure variation resulting in Li 'filament' formation within solid electrolytes, Nat. Mater. 20(11) (2021) 1485-1490.

[42] R. Raj, J. Wolfenstine, Current limit diagrams for dendrite formation in solid-state electrolytes for Li-ion batteries, Journal of Power Sources 343 (2017) 119-126.

[43] X. Ke, Y. Wang, G. Ren, C. Yuan, Towards rational mechanical design of inorganic solid electrolytes for all-solid-state lithium ion batteries, Energy Storage Mater. 26 (2020) 313-324.

[44] J.M. Naranjo, C.S. Martínez, B. Pandit, A. Várez, High performance NASICON ceramic electrolytes produced by tape-casting and low temperature hot-pressing: Towards sustainable all-solid-state sodium batteries operating at room temperature, J. Eur. Ceram. Soc. 43(11) (2023) 4826-4836.

[45] K. Min, High-Throughput Ab Initio Investigation of the Elastic Properties of Inorganic Electrolytes for All-Solid-State Na-Ion Batteries, J. Electrochem. Soc. 168(3) (2021) 030541.

[46] T. Wang, M. Zhang, K. Zhou, H. Wang, A. Shao, L. Hou, Z. Wang, X. Tang, M. Bai, S. Li, Y. Ma, A Hetero-Layered, Mechanically Reinforced, Ultra-Lightweight Composite Polymer Electrolyte for Wide-Temperature-Range, Solid-State Sodium Batteries, Adv. Funct. Mater. 33(22) (2023) 2215117.

[47] J. Wolfenstine, W. Go, Y. Kim, J. Sakamoto, Mechanical properties of NaSICON: a brief review, Ionics 29(1) (2022) 1-8.

[48] X. Wang, Z. Liu, Y. Tang, J. Chen, D. Wang, Z. Mao, Low temperature and rapid microwave sintering of $Na_3Zr_2Si_2PO_{12}$ solid electrolytes for Na-Ion batteries, J. Power Sources 481 (2021) 228924.

[49] D.J. Kalita, S.H. Lee, K.S. Lee, D.H. Ko, Y.S. Yoon, Ionic conductivity properties of amorphous Li–La–Zr–O solid electrolyte for thin film batteries, Solid State Ionics 229 (2012) 14-19.

[50] R. Murugan, V. Thangadurai, W. Weppner, Fast lithium ion conduction in garnet-type $Li_7La_3Zr_2O_{12}$, Angewandte Chemie International Edition 46(41) (2007) 7778.

[51] A.A. Shindrov, Increasing sinterability and ionic conductivity of $Na_3Zr_2Si_2PO_{12}$ ceramics by high energy ball-milling, Solid State Ionics 391 (2023) 116139.

[52] M. Niazmand, Z. Khakpour, A. Mortazavi, Electrochemical properties of nanostructure NASICON synthesized by chemical routes: A comparison between coprecipitation and sol-gel, J. Alloys Compd. 798 (2019) 311-319.

[53] J.S. Lee, C.M. Chang, Y.I. Lee, J.H. Lee, S.H. Hong, Spark plasma sintering (SPS) of NASICON ceramics, J. Am. Ceram. Soc. 87(2) (2004) 305-307.

[54] H. Wang, K. Okubo, M. Inada, G. Hasegawa, N. Enomoto, K. Hayashi, Low temperature-densified NASICON-based ceramics promoted by Na_2O-Nb_2O_5-P_2O_5 glass additive and spark plasma sintering, Solid State Ionics 322 (2018) 54-60.

[55] F. Lalère, J. Leriche, M. Courty, S. Boulineau, V. Viallet, C. Masquelier, V. Seznec, An all-solid state NASICON sodium battery operating at 200 °C, J. Power Sources 247 (2014) 975-980.

[56] J.A.S. Oh, L. He, A. Plewa, M. Morita, Y. Zhao, T. Sakamoto, X. Song, W. Zhai, K. Zeng, L. Lu, Composite NASICON ($Na_3Zr_2Si_2PO_{12}$) Solid-State Electrolyte with Enhanced Na^+ Ionic Conductivity: Effect of Liquid Phase Sintering, ACS applied materials & interfaces 11(43) (2019) 40125-40133.

[57] X.-L. Lin, Z.U.D. Babar, Y. Gao, J.-T. Gao, C.-X. Li, Influence of Triple Sintering Additives (BaO-CuO-B_2O_3) on the Sintering Behavior and Conductivity of the Proton-Conducting $BaZr_{0.1}Ce_{0.7}Y_{0.2}O_3$−δ Electrolyte Sintered at 1150 °C, ACS Applied Energy Materials 6(9) (2023) 4833-4843.

[58] Z. Yang, B. Tang, Z. Xie, Z. Zhou, NASICON-type $Na_3Zr_2Si_2PO_{12}$ solid‐state electrolytes for sodium batteries, ChemElectroChem 8(6) (2021) 1035-1047.

[59] Y. Li, Z. Sun, X. Yuan, H. Jin, Y. Zhao, NaBr-Assisted Sintering of $Na_3Zr_2Si_2PO_{12}$ Ceramic Electrolyte Stabilizes a Rechargeable Solid-state Sodium Metal Battery, ACS Appl. Mater. Interfaces 15(42) (2023) 49321-49328.

[60] K. Suzuki, K. Noi, A. Hayashi, M. Tatsumisago, Low temperature sintering of $Na_{1+x}Zr_2Si_xP_{3-x}O_{12}$ by the addition of Na_3BO_3, Scr. Mater. 145 (2018) 67-70.

[61] Y. Ji, T. Honma, T. Komatsu, Synthesis and Na^+ ion conductivity of stoichiometric $Na_3Zr_2Si_2PO_{12}$ by liquid-phase sintering with $NaPO_3$ glass, Materials 14(14) (2021) 3790.

[62] Y. Li, Z. Sun, H. Jin, Y. Zhao, Engineered Grain Boundary Enables the Room Temperature Solid-State Sodium Metal Batteries, Batteries 9(5) (2023) 252.

[63] W. Li, N. Zhao, Z. Bi, X. Guo, Insight into synergetic effect of bulk doping and boundary engineering on conductivity of NASICON electrolytes for solid-state Na batteries, Appl. Phys. Lett. 121(3) (2022) 033901.

[64] Z. Zhang, S. Shi, Y. Hu, L. Chen, Sol-gel synthesis and conductivity properties of sodium ion solid state electrolytes $Na_3Zr_2Si_2PO_{12}$, J. Inorg. Mater. 28 (2013) 1255-1260.

[65] L. Zhang, Y. Liu, J. Han, C. Yang, X. Zhou, Y. Yuan, Y. You, Al Doped into Si/P Sites of $Na_3Zr_2Si_2PO_{12}$ with Conducted Na_3PO_4 Impurities for Enhanced Ionic Conductivity, ACS Appl. Mater. Interfaces 15(38) (2023) 44867-44875.

[66] A. Ignaszak, P. Pasierb, R. Gajerski, S. Komornicki, Synthesis and properties of Nasicon-type materials, Thermochim. Acta 426(1-2) (2005) 7-14.

[67] H.-P. Hong, Crystal structures and crystal chemistry in the system $Na_{1+x}Zr_2Si_xP_{3-x}O_{12}$, Materials Research Bulletin 11(2) (1976) 173-182.

[68] R. Gordon, G. Miller, B. McEntire, E. Beck, J. Rasmussen, Fabrication and characterization of Nasicon electrolytes, Solid State Ionics 3 (1981) 243-248.

[69] U. von Alpen, M.F. Bell, W. Wichelhaus, Phase transition in nasicon ($Na_3Zr_2Si_2PO_{12}$), Materials Research Bulletin 14(10) (1979) 1317-1322.

[70] J.P. Boilot, J.P. Salanié, G. Desplanches, D. Le Potier, Phase transformation in $Na_{1+x}Si_xZr_2P_{3-x}O_{12}$ compounds, Materials Research Bulletin 14(11) (1979) 1469-1477.

[71] H. Park, M. Kang, Y. Park, K. Jung, B. Kang, Improving ionic conductivity of Nasicon ($Na_3Zr_2Si_2PO_{12}$) at intermediate temperatures by modifying phase transition behavior, J. Power Sources 399 (2018) 329-336.

[72] P.W. Jaschin, C.R. Tang, E.D. Wachsman, High-rate cycling in 3D dual-doped NASICON architectures toward room-temperature sodium-metal-anode solid-state batteries, Energy Environ. Sci. 17(2) (2024) 727-737.

[73] A.G. Jolley, G. Cohn, G.T. Hitz, E.D. Wachsman, Improving the ionic conductivity of

NASICON through aliovalent cation substitution of $Na_3Zr_2Si_2PO_{12}$, Ionics 21 (2015) 3031-3038.

[74] Y. Lu, L. Li, Q. Zhang, Z. Niu, J. Chen, Electrolyte and Interface Engineering for Solid-State Sodium Batteries, Joule 2(9) (2018) 1747-1770.

[75] G. Yan, S. Yu, J.F. Nonemacher, H. Tempel, H. Kungl, J. Malzbender, R.-A. Eichel, M. Krüger, Influence of sintering temperature on conductivity and mechanical behavior of the solid electrolyte LATP, Ceram. Int. 45(12) (2019) 14697-14703.

[76] Y. Kim, H. Jo, J.L. Allen, H. Choe, J. Wolfenstine, J. Sakamoto, G. Pharr, The Effect of Relative Density on the Mechanical Properties of Hot‐Pressed Cubic $Li_7La_3Zr_2O_{12}$, J. Am. Ceram. Soc. 99(4) (2016) 1367-1374.

[77] J. Lee, C. Zhao, C. Wang, A. Chen, X. Sun, K. Amine, G.L. Xu, Bridging the gap between academic research and industrial development in advanced all-solid-state lithium–sulfur batteries, Chemical Society Reviews (2024).

[78] K. Hiraoka, M. Kato, T. Kobayashi, S. Seki, Polyether/$Na_3Zr_2Si_2PO_{12}$ composite solid electrolytes for all-solid-state sodium batteries, The Journal of Physical Chemistry C 124(40) (2020) 21948-21956.

[79] Y. Dong, P. Wen, H. Shi, Y. Yu, Z.S. Wu, Solid‐State Electrolytes for Sodium Metal Batteries: Recent Status and Future Opportunities, Advanced Functional Materials 34(5) (2024) 2213584.

[80] F. Yang, E. Campos dos Santos, X. Jia, R. Sato, K. Kisu, Y. Hashimoto, S.-i. Orimo, H. Li, A dynamic database of solid-state electrolyte (DDSE) picturing all-solid-state batteries, Nano Materials Science 6(2) (2024) 256-262.